Role of Ionic Strength on the Relationship of Biopolymer Conformation, DLVO Contributions, and Steric Interactions to Bioadhesion of *Pseudomonas putida* KT2442

Nehal I. Abu-Lail and Terri A. Camesano*

Department of Chemical Engineering, Worcester Polytechnic Institute, 100 Institute Rd., Worcester, Massachusetts 01609

Received February 23, 2003; Revised Manuscript Received April 25, 2003

Biopolymers produced extracellularly by *Pseudomonas putida* KT2442 were examined via atomic force microscopy (AFM) and single molecule force spectroscopy. Surface biopolymers were probed in solutions with added salt concentrations ranging from that of pure water to 1 M KCl. By studying the physicochemical properties of the polymers over this range of salt concentrations, we observed a transition in the steric and electrostatic properties and in the conformation of the biopolymers that were each directly related to bioadhesion. In low salt solutions, the electrophoretic mobility of the bacterium was negative, and large theoretical energy barriers to adhesion were predicted from soft-particle DLVO theory calculations. The brush layer in low salt solution was extended due to electrostatic repulsion, and therefore, steric repulsion was also high (polymers extended 440 nm from surface in pure water). The extended polymer brush layer was "soft", characterized by the slope of the compliance region of the AFM approach curves (−0.014 nN/nm). These properties resulted in low adhesion between biopolymers and the silicon nitride AFM tip. As the salt concentration increased to ≥0.01 M, a transition was observed toward a more rigid and compressed polymer brush layer, and the adhesion forces increased. In 1 M KCl, the polymer brush extended 120 nm from the surface and the rigidity of the outer cell surface was greater (slope of the compliance region = −0.114 nN/nm). A compressed and more rigid polymer layer, as well as a less negative electrophoretic mobility for the bacterium, resulted in higher adhesion forces between the biopolymers and the AFM tip. Scaling theories for polyelectrolyte brushes were also used to explain the behavior of the biopolymer brush layer as a function of salt concentration.

Introduction

The presence and physicochemical properties of biopolymers on the surface of a bacterium are known to influence bioadhesion to surfaces including soil,[1−3] biomaterials such as endotracheal tubes,[4] and mammalian cells.[5] Bacterial adhesion and biofilm formation have applications in a number of engineering, scientific, and medical disciplines.

The initial adhesion of a microbe to a surface was suggested to be controlled by electrostatic and van der Waals interactions,[6] as could be modeled by the classical Derjaguin−Landau−Verwey−Overbeek (DLVO) theory of colloidal stability.[7] Bulk investigations of bacterial attachment to a similarly charged surface show that ionic strength usually affects the attachment probability, with less attachment seen in low ionic strength solutions because of increased long-range electrostatic repulsion.[8] According to DLVO theory, increasing the solution's ionic strength should monotonically decrease the long-range repulsion between a negatively charged bacterium and a negatively charged surface. There have been a few cases where the expected trend with ionic strength was not seen. For example, cell adhesion or flocculation was seen at a finite salt concentration despite predictions of energy barriers that should have been too large to permit adhesion/flocculation[9,10] or bacterial adhesion was indifferent to electrolyte concentration.[10−12] One contributing factor to this discrepancy between bacterial attachment and model predictions involves bacterial motility, because the rotation of the flagella of *Escherichia coli* in solutions with low ionic strength (0.02 M phosphate buffer) was found to provide sufficient energy to assist in attachment.[13] The increased adhesion was attributed to faster transport of motile cells toward the surface or the use of the flagella as an anchor to tether the bacteria to the surface. Another explanation that has been suggested is charge regulation. A recent modeling effort explained that weakly charged groups on the bacterial surface are involved in an equilibrium process by which they exchange between associated and dissociated states,[14] and this charge regulation gives rise to a nonmonotonic decrease in the repulsion between like-charged colloids with decreasing cell−substrate separation. In some cases charge regulation can lead to a regime of *increased* repulsion at higher salt concentrations. Poortinga et al. recently provided evidence that charge transfer is an important part of bacterial adhesion and that bacteria with a thicker ion-penetrable layer adhere to a greater extent onto a similarly charged substrate.[11] Flagellar rotation, charge regulation, and ion penetrability are important effects that are not typically addressed by

* To whom correspondence should be addressed. Telephone: 508-831-5380. Fax: 508-831-5853. E-mail: terric@wpi.edu.

10.1021/bm034055f CCC: $25.00
Published on Web 05/30/2003

DLVO theory. Additional factors also contribute to the discrepancy between the prediction and observation of bacterial adhesion as a function of ionic strength, particularly for microbes with substantial extracellular polymer layers.

For charged polymers on bacterial surfaces, the solution ionic strength will change the conformation and adhesion behavior of these macromolecules, as well as changing the "softness" of the polymer brush layer, each in ways that cannot be fully described by classical DLVO or extended DLVO theories.[15] By viewing the biopolymer as a polyelectrolyte brush layer, the properties of the macromolecules in the brush layer can be characterized using polyelectrolyte scaling relationships.

Recent advances in the application of analytical techniques to microbial systems, such as through single-molecule force spectroscopy (SMFS),[16,17] atomic force microscopy (AFM),[18−22] total internal reflection aqueous fluorescence microscopy,[23] or other optical trapping/evanescent wave techniques,[24] make it possible to probe the molecular components of the microbial adhesion process.

We chose *Pseudomonas putida* KT2442 as a model polysaccharide-producing microorganism, a strain for which we already had some information on surface properties. For example, this microbe is fairly hydrophilic, based on a water contact angle of $24.5 \pm 3.4°$,[25] is negatively charged, and has a very low isoelectric point (2.3), indicating that the surface consists of anionic polysaccharides with phosphate and/or carboxylic group moieties.[26] Previous AFM studies of *P. putida* KT2442 demonstrated that the extracellular biopolymers were heterogeneous in terms of elastic properties, contour lengths, and adhesion affinities for silicon nitride.[27] The biopolymers were flexible in all solvents studied (water, methanol, formamide, and 0.1 M KCl), based on application of the freely jointed chain model to polymer stretching data.[17] Two studies demonstrated that ionic strength only slightly affected the adhesion affinities or interaction forces between *P. putida* KT2442 biopolymers and silicon nitride (from water to 0.01 M KCl[17] or from 0.01 to 100 mM MOPS buffer[26]). We hypothesized that the lack of a substantial effect of the ionic strength on the observed interaction forces or adhesion affinities was due to the fact that at the ionic strengths tested, the concentration of bulk ions was not great enough to counterbalance the ion concentration in the polyelectrolyte brush layer surrounding the microbes.

The current study provides a more thorough and systematic investigation of the role of ionic strength on the physiochemical properties of biopolymers on the surface of *Pseudomonas putida* KT2442. Solutions with a wider range of salt concentrations were chosen, including solutions with much higher salt concentrations than had been previously studied (from pure water to 1 M KCl). For each solution studied, the interaction forces during the approach of a silicon nitride AFM tip to the bacterium were measured, as well as the adhesive forces after the two had been in contact. Direct interaction force measurements were compared with energy predictions based on soft-particle DLVO theory calculations. A steric model for polymer brushes was applied to probe the changing conformation of the brush layer as a function of ionic strength. Physicochemical properties of the polymers such as the Kuhn and contour lengths were characterized by applying polymer statistical models. The brush layer thickness and density were correlated with salt concentration using scaling models for polyelectrolytes at solid/liquid interfaces. Biopolymer conformation and steric/electrostatic properties were correlated with bioadhesion as a function of salt concentration.

Materials and Methods

Bacterial Culture Preparation. Our work focused on *Pseudomonas putida* KT2442, which produces a cellulose-like EPS.[27] *P. putida* KT2442 can be found in soil, freshwater, and the rhizospheres of agriculturally important plants[28,29] and can degrade chlorinated benzenes.[30−33] It is a soil microorganism and a wealth of information is available regarding its genetic[28,29] and physicochemical properties.[17,25−27] KT2442 cultures were grown in M9 buffer containing a mineral salt mixture supplemented with 5mM benzoate and 50 μg/L rifampicin.[25]

Electrophoretic Mobility. The electrophoretic mobility of *P. putida* KT2442 was measured using a zeta potential analyzer (Zeta PALS, Brookhaven). Measurements were performed three times and averaged, on late-exponential phase bacterial cells resuspended in KCl solutions of varying ionic strengths (10^{-3} −0.15 M KCl; pH = 8.0).

Preparing Bacterial Samples for AFM Work. Glass slides were cleaned by soaking in a 3:1 HCl/HNO_3 solution for 25 min followed by copious rinsing in deionized (DI) water. This step was followed by soaking in 4:1 H_2SO_4/H_2O_2 solution for 25 min, rinsing in DI water, and storage of the slides in a beaker of water that had been sterile-filtered through a 0.2 μm syringe filter until use. KT2442 cells were covalently bonded to clean, silanized glass slides, as described elsewhere.[26] The bonding protocol involves immobilization of bacteria using the zero-length cross-linker 1-ethyl-3-(3−dimethylaminopropyl)carbodiimide (EDC), stabilized by sulfo-hydroxysuccinimide (sulfo-NHS). The zero-length cross-linkers modify amino acid side groups (on the glass slide) to permit cross-link formation, but they do not remain as part of the linkage nor do they modify the bacterial surface. Prior research on pure polymers suggests that the main effect of the EDC/NHS concentration is to change the structure and density of the polymer layer being formed, which would change the observed interaction forces.[34] However, we always have much less than a monolayer of bacteria attached to the slide, and so the EDC/NHS treatment should not affect the observed interaction forces. Prior work has also shown that biological activities are not disrupted by these chemicals when used in similar bonding protocols.[35,36] After the bonding reaction, slides were transferred to a petri dish containing the desired solvent (water or a KCl solution).

Force Analysis Using AFM. Forces were measured between hydrated individual bacterial cells and silicon nitride cantilevers using an AFM (Digital Instruments Dimension 3100 with Nanoscope III controller). Silicon nitride tips were purchased from Digital Instruments (DNPS tips). The spring constant for these tips was 0.13 ± 0.02 N/m, measured using the Cleveland method[37] and the correlation equations given

in the Digital Instruments software. The tips were cleaned just prior to use by exposure to ozone generated by ultraviolet light irradiation in an oxygen atmosphere for 1 min, which removes any organic carbon contamination covering the tip apex.[38] To select a cell for analysis, an image was obtained in the tapping mode of a portion of the glass slide. The tip was then positioned over the center of a bacterium, the rastering of the cantilever was stopped, the tapping was turned off, and a force measurement was performed. At least five measurements were performed on a single area of a bacterial cell, and such measurements were performed on at least five bacteria for a given salt solution. Forces were recorded while the tip approached and was retracted from the sample.

The data files were treated as described previously[26] to convert cantilever deflection to force, using the constant compliance region of the curves to "zero" the force curves.[39] Although the method used to determine the origin of the force curves was developed for hard silica spheres, these principles can be applied to other colloidal particles such as soft biological cells and fibrous materials,[39] as has been successfully done in many cases.[21,40−44] In addition, Boulbitch et al. recently proved through theoretical relations that the deformation of the envelope of a gram-negative bacterium from a force-displacement relation measured on the top of the bacterium is accurately approximated by a linear dependence,[45] suggesting that nonelastic components of the force do not limit our ability to specify the origin of each force−distance relationship. In our study, force measurements were made on clean glass before and after force measurements on bacterial cells, to ensure that the tip was not contaminated during the course of the experiment. The measurements on glass were always practically identical, confirming that no biopolymers remained on the tip after a force measurement.

Determination of Polymer Brush Layer Thickness. A model developed for grafted polymers at relatively high surface coverage was used to model steric interactions between the AFM tip and cell surface polymers. The force per unit area between two surfaces, F_{St}, only one of which is coated with polymer, has been modeled following the work of Alexander[46] and de Gennes.[47] This model was modified by Butt et al.[48] to describe the forces between a spherical AFM tip and a flat surface by integrating the force per unit area over the tip surface, to produce the interaction force

$$F_{St} = 50k_BTa_1L\Gamma^{3/2}e^{-2\pi h/L} \quad (1)$$

where k_B is Boltzmann constant, T is temperature, a_1 is the tip radius, Γ is the grafted polymer density in the brush layer (m^{-2}) and reflects how much of the surface is covered by polymers, h is the distance between the two surfaces, and L is the equilibrium height of the polymer brush layer. For these calculations, the tip radius was assumed to be 250 nm based on a previous demonstration that these tips interact as spheres with radii between 100 and 400 nm.[49,50]

Calculation of Surface Potential for Soft Particles. Recent work suggested that for soft particles, such as bacteria, the zeta potential is not an accurate measure of surface potential.[12,51−53] Therefore, soft-particle DLVO theory was used to evaluate the electrostatic interactions between *P. putida* KT2442 and silicon nitride. This theory assumes the presence of an ion-penetrable, charged polyelectrolyte layer around a rigid core.[53] The approximate mobility formula for soft particles[13,51,52,54,55] is expressed as

$$\mu = \frac{\epsilon_o\epsilon}{\eta}\frac{\Psi_o/K_m + \Psi_{DON}/\lambda_s}{1/Km + 1/\lambda_s} + \frac{eZN}{\eta\lambda_s^2} \quad (2)$$

where ϵ is the permittivity of a vacuum and ϵ_o is the relative permittivity of the solvent, Ψ_o is the surface zeta potential, K_m is the Debye−Hückel parameter for the polymer layer, Ψ_{DON} is the Donnan potential of the polymer layer, Z is the valence of the charged groups in the polymers, e is the electron charge, N is the density of the charged groups, and λ_s is the softness parameter, which has dimensions of reciprocal length. The parameters K_m, Ψ_o, and Ψ_{DON} are all functions of ionic strength.[53] The expressions for determining these parameters are provided in the Appendix.

Calculation of Interaction Energies. DLVO interaction energy profiles between the bacterium and silicon nitride were calculated. Bacterium/AFM tip interactions were treated using sphere−sphere geometry. The total DLVO interaction energy (E_t) between the bacterium and the silicon nitride tip was calculated as the sum of London−van der Waals and electrostatic interactions[56]

$$E_t = E_e + E_v \quad (3)$$

where E_e is the electrostatic energy and E_v is the interaction energy due to London−van der Waals forces. The electrostatic interactions were calculated using the linearized version of the Poisson−Boltzmann expression[56]

$$E_e = \frac{2\pi a_1a_2nk_BT}{(a_1+a_2)\kappa^2}(\Phi_1^2+\Phi_2^2)\left(\frac{2\Phi_1\Phi_2}{\Phi_1^2+\Phi_2^2}\ln\left(\frac{1+\exp(-\kappa h)}{1-\exp(-\kappa h)}\right)+\ln[1-\exp(-2\kappa h)]\right) \quad (4)$$

where a_2 is the radius of the bacterium, Φ_1 and Φ_2 are the reduced potentials of tip and the bacterium, respectively, which relate to their surface potentials ψ_1 and ψ_2 according to $\Phi = ze\psi/k_BT$.[56]

For bacterial cells, the soft-particle potential (Ψ_o) calculated from eq 3 was used as the surface potential (ψ). For the silicon nitride tip, the surface potential was taken to be the zeta potential, based on applying the Smoluchowski expression[57] to electrophoretic mobility values obtained from the literature.[58,59]

The van der Waals interaction energy between two dissimilar spheres was calculated using a Hamaker expression, corrected for retardation effects[60]

$$E_v = -\frac{-Aa_1a_2}{6h(a_1+a_2)(1+11.12h/\lambda_c)} \quad (5)$$

where A is the Hamaker constant for the interacting media and λ_c is the "characteristic wavelength" of the interaction,

often assumed to be 100 nm. A value of 10^{-20} J was used for the Hamaker constant describing bacterial−silicon nitride interactions in water, using a value previously developed for the interactions between *Pseudomonas aeruginosa* and glass.[61] This is a reasonable approximation because the zeta potentials and water contact angles of *P. putida* and *P. aeruginosa* are very similar. The water contact angles for both strains indicate hydrophilic surfaces and are 24.5 ± 3.4° (26) and 33.5 ± 1.2° (62) for *P. putida* and *P. aeruginosa*, respectively. The zeta potentials of *P. putida* and *P. aeruginosa* are −17.31 ± 0.06[17] and −17.59 mV,[62] respectively. In addition, we have previously shown that interaction profiles in bacterium-glass systems are similar to those in bacterium-silicon nitride systems.[12]

Polymer Elastic Properties. The freely jointed chain model was applied to the force-extension data of AFM retraction curves to estimate the Kuhn lengths (l_k). In the freely jointed chain (FJC) model, the polymer is considered to be composed of independent rigid segments, each of length l_k, and connected by freely rotated pivots with equal probabilities for rotation in all directions. The chain gets more flexible as the Kuhn length gets smaller. The force needed to stretch a FJC to a length h is given by[63−64]

$$F_{\text{chain}} = \frac{-k_B T}{l_k}\mathbf{L}^{-1}\left(\frac{h}{l_c}\right) \tag{6}$$

where k_B is the Boltzmann constant, T is the absolute temperature, l_c is the contour length of the portion of the chain that was stretched, and $\mathbf{L}^{-1}$ is the inverse Langevin function, approximated by the first four terms of its series

$$\mathbf{L}^{-1}\left(\frac{h}{l_c}\right) = 3\left(\frac{h}{l_c}\right) + \frac{9}{5}\left(\frac{h}{l_c}\right)^3 + \frac{297}{175}\left(\frac{h}{l_c}\right)^5 + \frac{1539}{875}\left(\frac{h}{l_c}\right)^7 \tag{7}$$

Scaling Relationships for Polyelectrolyte Brushes. Considerations of tethered polyelectrolytes based on self-consistent field theory[65] predict a roughly parabolic segment density profile that extends further with increasing charge density or decreasing salt concentration.[66,67] For many cases, simpler scaling relations can be used to describe the behavior of polyelectrolyte brushes. In this study, the effects of added salt concentration on the dimensions of the biopolymer brush layer were predicted using scaling theories developed for grafted brushes of polyelectrolytes. Available theories characterize the brush layer by relating the changes in the brush height (L), polymer grafting density (Γ), contour length (L_c), and Kuhn length (l_k) to the salt concentration of the solvent (C_s).[68−73] The contour length is in turn related to the brush height. For the purpose of these scaling calculations, we assumed that the polymer contour length would be related to the brush height, and the relationship $L_c = 1.25L$ was used. We could not use the l_c values estimated from application of the FJC model because these "contour lengths" (l_c values) represent the contour length of some region of the polymer chain that was stretched. The AFM tip may have come into contact with the polymer chain anywhere along its length (i.e., not necessarily at the end), and these contour length values will most likely represent the lengths of short sections of the chains, rather than the whole chain molecules. The arbitrary factor that we assumed (1.25) affects only the values of the constants in the scaling relations, and does not affect the observed relationships between contour length, density, Kuhn length, and salt concentration.

For uncharged brushes, scaling theories predict that the brush layer height is proportional to $\Gamma^{1/3}$.[46] The behavior of charged brushes deviates substantially from this relationship, especially at low ionic strengths. To account for the behavior of charged brushes, electrostatic blob models were developed.[72,74,75] Blob models account for excluded volume effects resulting from chain expansions due to interactions between the charged chains (electrostatic, van der Waals, and steric), and some blob models can also be made to account for the elasticity of the biopolymers. For polyelectrolytes, the brush layer thickness was related to the excluded volume (υ) and segment length (l_k) through the relation $L \sim L_c(\upsilon\Gamma/l_k)^{1/3}$. The excluded volume interaction parameter accounts for chain interactions. A version of the Daoud−Cotton model that was corrected for polymers attached to a spherical surface was used to calculate the excluded volume parameter[70]

$$\left(\frac{L}{a_2} + 1\right)^{5/3} = 1 + \frac{KL_c}{a_2}\left(\frac{\upsilon\Gamma}{l_k}\right)^{1/3} \tag{8}$$

where K is a constant whose value is close to unity. Values of l_k were obtained via application of the FJC model to the AFM retraction curves, where an average l_k value was found for each added salt concentration. L and Γ were obtained from applying the steric model (eq 1) to AFM approach curves.

Several models have been proposed to relate the brush layer height to salt concentration, each with the general form $L \sim C_s^{-m}$,[70] where m is a fractional exponent. Pincus suggested that chain stiffening could be ignored or that the Kuhn length is equal to that of an equivalent uncharged chain. In this case and for a semidilute solution, the layer thickness was related to salt concentration as $L \sim C_s^{-1/3}$.[76] Zhulina et al. developed relations for salted and unsalted brushes based on the sum of electrostatic and nonelectrostatic forces, in which $L \sim L_c\Gamma^{1/3}C_s^{-1/3}$ for the salted brush.[68,73] The electrostatic wormlike chain model was developed for the case where chain stiffening occurs or the Kuhn length changes as the salt concentration in solution is modified.[77−79] The electrostatic WLC model predicts the scaling relation $L \sim C_s^{-1/2}$. Each model was tested for its ability to describe the relationship between brush layer height and salt concentration.

Results

Biopolymer Electrostatic Properties and Predicted Energy Barriers to Attachment Based on Soft-Particle DLVO Theory. The electrophoretic mobility of *P. putida* KT2442 reached a nonzero asymptotic value as the salt concentration increased (Figure 1), which is characteristic of "soft" particles.[53] We applied the soft-particle DLVO theory[51−53,80] to our electrophoretic mobility data as a function of ionic strength, and determined that $ZN = -0.072$ M and $1/\lambda = 1$ nm. These values are similar to ones reported for *Nitrosomonas europaea* and *Escherichia coli* IFO-3301.[53] Using the soft-cell potentials, the total interaction energy

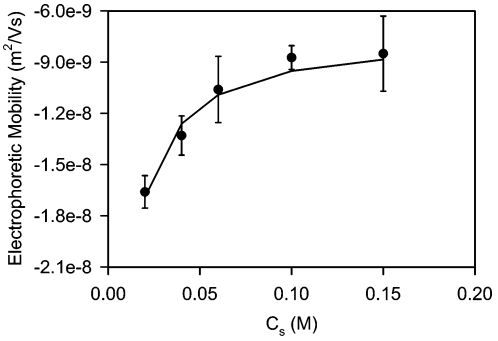

Figure 1. Electrophoretic mobility of *P. putida* KT2442 as a function of added salt concentration. Each point represents an average of three experimental measurements (pH = 8.0), whereas the line is the fit of these data points to soft-particle DLVO theory (eq 2, $R^2 = 0.97$).

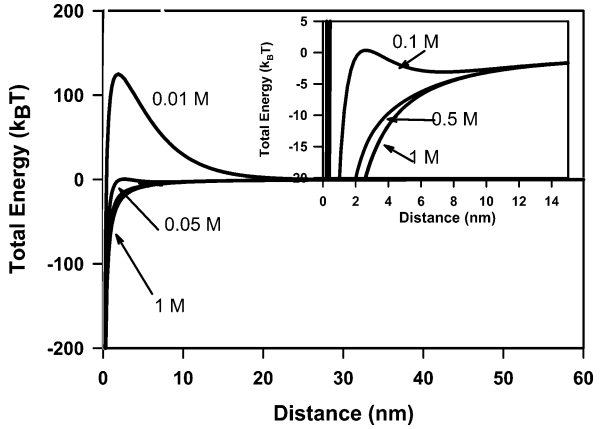

Figure 2. Total interaction energy between the silicon nitride AFM tip and *P. putida* KT2442 cells, based on soft-particle DLVO theory calculations (electrostatic and van der Waals interactions). The interactions were calculated based on sphere−sphere geometry, where $a_1 = 250$ nm, $a_2 = 500$ nm, $A = 10^{-20}$ J.[61] The surface potentials for the tip and bacterium are summarized in Table 1.

Table 1. Summary of Parameters for DLVO Interaction Energy Calculations

C_s (M)[a]	ψ_{tip} (mV)	$\psi_{bacteria}$ (mV)	E_{max} (k_BT)
0.01	−16	−31.7	125
0.05	−14	−9.2	1.45
0.1	−12	−4.6	all attraction
0.5	−10	−3.0	all attraction
1	−8	−3.0	all attraction

[a] C_s is the added salt concentration, ψ_{tip} is the surface potential of the tip as estimated by conventional zeta potential theory, $\psi_{bacteria}$ is the surface potential of the bacteria estimated from soft-particle DLVO theory (eq 3), and E_{max} is the calculated energy barrier based on DLVO theory (eq 7).

between the tip and the bacterium was calculated as a function of added salt concentration (Figure 2, Table 1). At salt concentrations <0.05 M, repulsion was observed between the bacterium and the tip. However, at salt concentrations >0.05 M, attraction was always observed between the bacterium and the tip.

Although an attempt was made to use the extended-DLVO model (accounting for acid−base interactions), this approach was discarded because it produced unrealistically high repulsive energy barriers at short separation distances (data not shown). These energy barriers of 100's of k_BT's were present at all salt concentrations tested, even though experiments indicated that adhesion occurred at an appropriately high salt concentration. The use of conventional-DLVO theory, modified to account for the behavior of "soft" particles, produced predictions that were closest to experimental evidence of adhesion.

Biopolymer Conformation

Thickness of the Polymer Brush Layer. The presence of bacterial polymers caused steric repulsion between the bacterium and the tip. These forces were quantified using the Alexander and de Gennes models for steric interactions between a grafted polymer layer and a bare surface, as modified by Butt et al. when the "surface" is a rounded AFM tip (eq 1)[46−48] (Figure 3). The height of the brush layer decreased with increasing salt concentration (Table 2). The grafting density increased with increasing C_s, whereas the total amount of biopolymer on the bacterial surface (estimated as ΓL) was nearly constant and not dependent on C_s. Bacterial cells were always grown under the same conditions, and therefore, the total amount of polymer should not have changed when the final suspension solution was changed.

Elastic Properties of the Biopolymers. The biopolymer layer on the surface of KT2442 undergoes changes in its conformation that are dependent upon the salt concentration in solution. In low ionic strength solutions, the polymer brush layer is most extended ($L = 440$ nm). This extension results in the surface of the bacterium appearing as "soft". When the salt concentration increased, the biopolymer brush layer collapsed onto the cell membrane, as evidenced by the decreasing values of L.

The slope of the compliance region of the AFM approach curves provides corroborating evidence of this transition in cell softness. This slope represents the amount that the AFM tip could be compressed into the polymer layer. The value of the slope decreased from −0.014 to −0.114 nN/nm as the salt concentration increased from that of pure water to 1 M KCl (Figure 3, Table 2), indicating that the surface was more compliant in lower salt solutions.

On a microscopic basis, the biopolymers were flexible in all salt solutions studied, as modeled using the freely jointed chain model. The Kuhn lengths ranged from 0.154 to 0.65 nm in all solutions (Figure 4). In a previous study, we reported the range of Kuhn lengths for these biopolymers in water, 0.01 and 0.1 M KCl. The average values here are in the middle of the ranges we reported previously.[17] Statistical tests confirmed that l_k in water was significantly different from l_k in all other salt solutions. However, the l_k values in all salt solutions except water were not statistically significantly different from one another. All statistical analyses were based on the Dunn rank sum test ($p > 0.05$).

Scaling Relations. The brush layer height can be correlated with $\Gamma^{1/3}$ for an uncharged brush.[46] To maintain dimensionless numbers, we compared L/l_k vs $(\Gamma l_k^2)^{1/3}$, but this scaling relationship was not satisfactory for our data (Figure 5A). An alternate relationship for a polyelectrolyte brush[72,74,75] was applicable (Figure 5B). In the latter model, L is correlated with $L_c(\Gamma\upsilon)^{1/3}l_k^{-1/3}$. The polyelectrolyte model accounts for excluded volume interactions between adjacent "blobs" of the polymer chain and also accounts for the elastic properties of the polymers. The validity of the polyelectrolyte

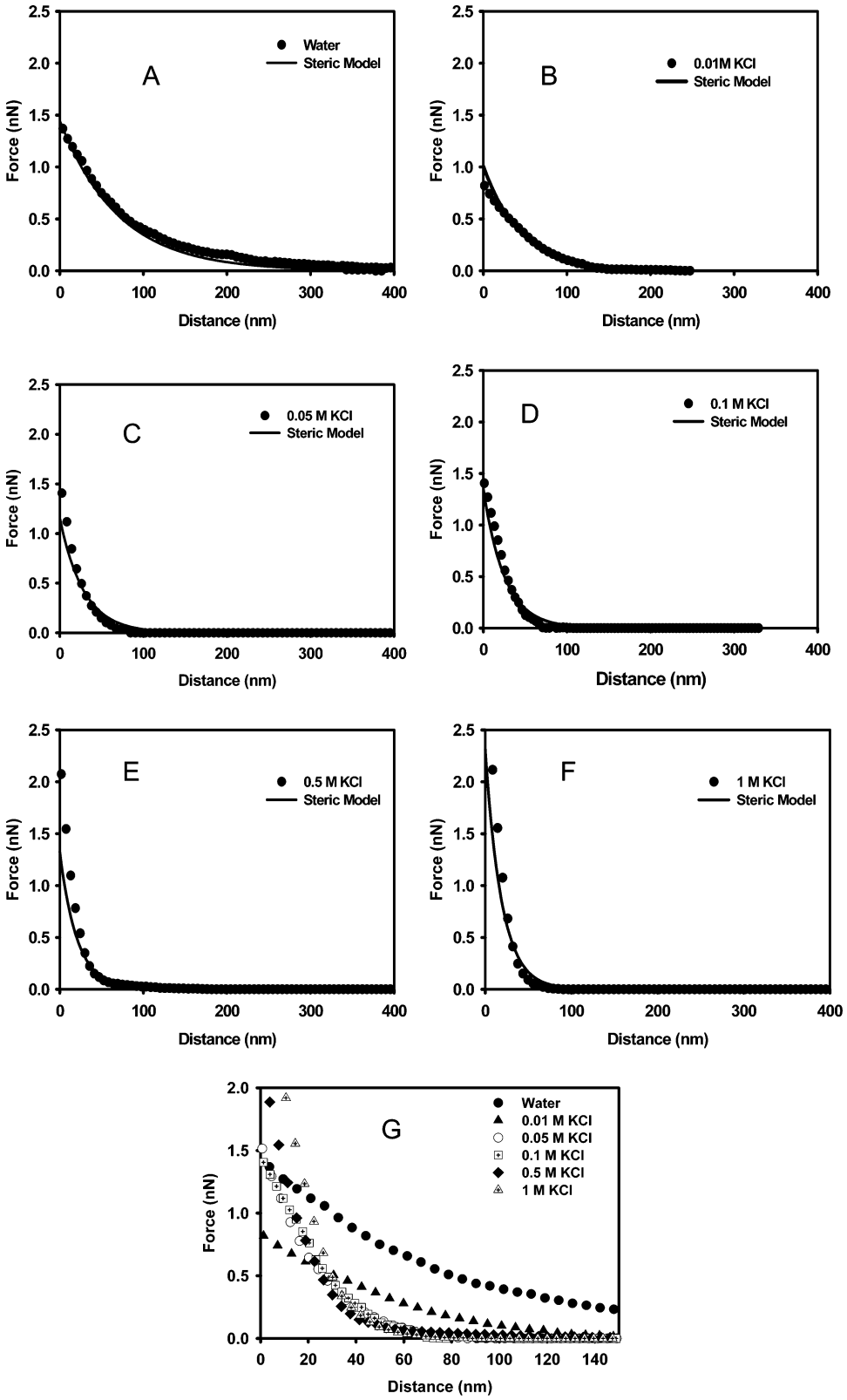

Figure 3. Summary of the average AFM approach curves for *P. putida* KT2442 in different salt solutions. (A) Water, (B) 0.01 M KCl, (C) 0.05 M KCl, (D) 0.1 M KCl, (E) 0.5 M KCl, (F) 1 M KCl, and (G) A comparison between average approach curves in all salt solutions. In plots A−F, the symbols represent experimental data and the solid lines are best fits based upon the steric model (eq 1). Steric model results and the slopes of the compliance regions are given in Table 2.

scaling relationship confirms that the polymer brush layer on the surface of *P. putida* KT2442 is charged.

Scaling relationships for polyelectrolytes can also be used to determine the relationship between the brush height (L) and the salt concentration (C_s). Several models have been proposed for this relationship and are based on Monte Carlo simulations,[81] mean field calculations,[72,75] and self-consistent field theories.[66,73] For *P. putida* KT2442, the dependence of the brush layer height on the added salt concentration was investigated through application of the general power law

Table 2. Physical Properties of Brush Layer as a Function of Salt Concentration

C_s[a] (M KCl)	L (nm)	$\Gamma \times 10^{-15}$ (molecules/m^2)	$L\Gamma \times 10^{-8}$ (molecules/m)	R^2 for steric model	slope of compliance region (nN/nm)	l_k (nm)	average adhesion force (nN)
water[b]	440	1.6	7.04	0.99	−0.014	0.208	−0.33
0.01	280	1.7	4.76	0.99	−0.010	0.202	−0.46
0.05	180	2.5	4.50	0.95	−0.054	0.205	−0.60
0.1	160	3.0	4.80	0.98	−0.035	0.200	−0.66
0.5	130	3.4	4.42	0.98	−0.109	0.186	−1.04
1.0	120	5.2	6.24	0.98	−0.114	0.180	−1.85

[a] C_s is the added salt concentration, L is the brush thickness, Γ is the grafting density of the polymer brush, l_k is the Kuhn length estimated by the use of FJC model (eq 10). [b] Although the solvent was pure water, we estimated that the salt concentration with the polymer in solution was 0.0027 M. This estimate was based on extension of the line in Figure 6A and extrapolation of the salt concentration at a brush layer thickness of 440 nm.

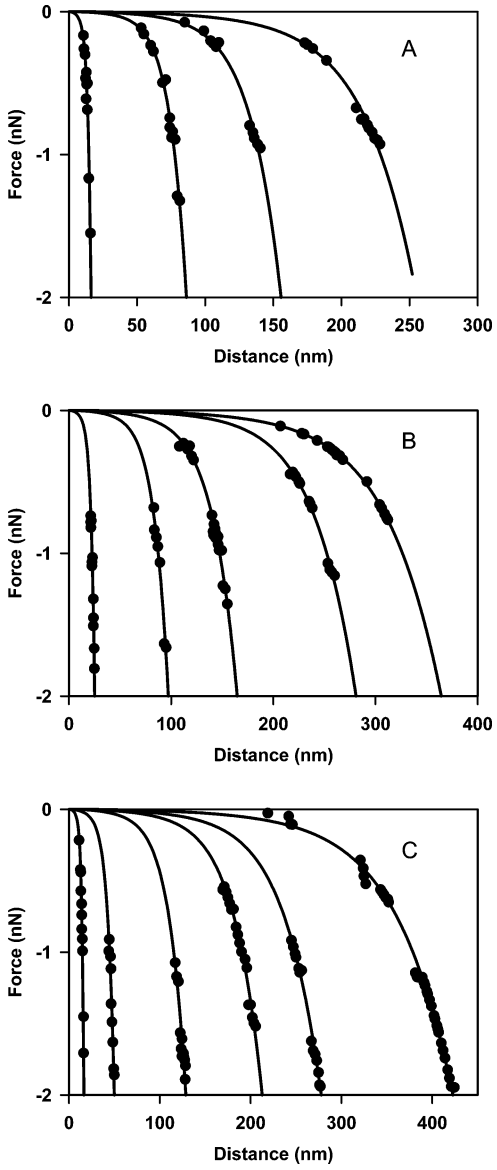

Figure 4. Representative data and modeling results for the application of the freely jointed chain model (eq 10) to AFM retraction curves. Although hundreds of chains were examined, we present representative data for a few chains. The model fit the chains equally well in all experiments. Experimental conditions were as follows: (A) 0.05 M KCl, estimated L_c (nm), l_k (nm), and R^2 values for the chains from left to right are (11, 0.154, 0.93), (54, 0.247, 0.97), (102, 0.184, 0.99), and (172, 0.154, 0.98). (B) 0.5 M KCl, estimated L_c (nm), l_k (nm), and R^2 values for the chains from left to right are (17, 0.154, 0.96), (63, 0.195, 0.96), (111, 0.154, 0.98), (183, 0.193, 0.99), and (245, 0.155,1.0). (C) 1.0 M KCl, estimated L_c (nm), l_k (nm), and R^2 values for the chains from left to right are (10, 0.245, 0.97), (36, 0.154, 0.99), (86, 0.165, 0.97), (143, 0.154, 0.98), (187, 0.154, 0.99), and (285, 0.154, 1.0).

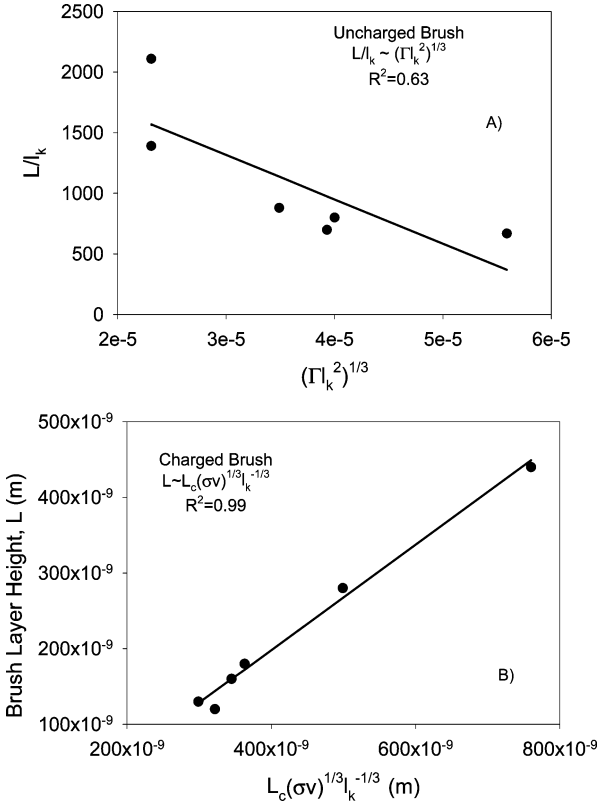

Figure 5. Application of scaling theories for polyelectrolyte brushes. (A) The scaling results for an uncharged brush. (B) The scaling relation for a charged polyelectrolyte brush. In A and B, symbols are experimental values (or calculated values based on experimental data) and the lines are best fits. The excluded volume was estimated using eq 12. The steric model was applied to the data in Figure 3 to obtain the values of Γ. The Kuhn lengths were estimated from application of the freely jointed chain model to the data in Figure 4.

formula $L \sim C_s^{-m}$.[70] The exponent that best represented our data was $m = -0.51$ (Figure 6), which was practically the same as the scaling relation predicted for an electrostatic wormlike chain in a dilute solution ($L \sim C_s^{-1/2}$), where chain stiffening causes l_k to change with salt concentration.[77,78,82] The other relationships predict that $L \sim C_s^{-1/3}$ for a salted brush in the regime where added salt far exceeds the counterion concentration[73] or $L \sim C_s^{-2/3}$ in an alternate model to account for local chain stiffening and excluded volume effects.[75] Although the exponent $m = -0.51$ provided the best correlation with our data, all of the models to relate L and C_s fit the data well. We therefore cannot conclusively distinguish between these three models.

We used one of the models (the electrostatic WLC) to also determine the maximum compression of the brush layer (L_o), which was found to be 105 nm (Figure 6A). If we con-

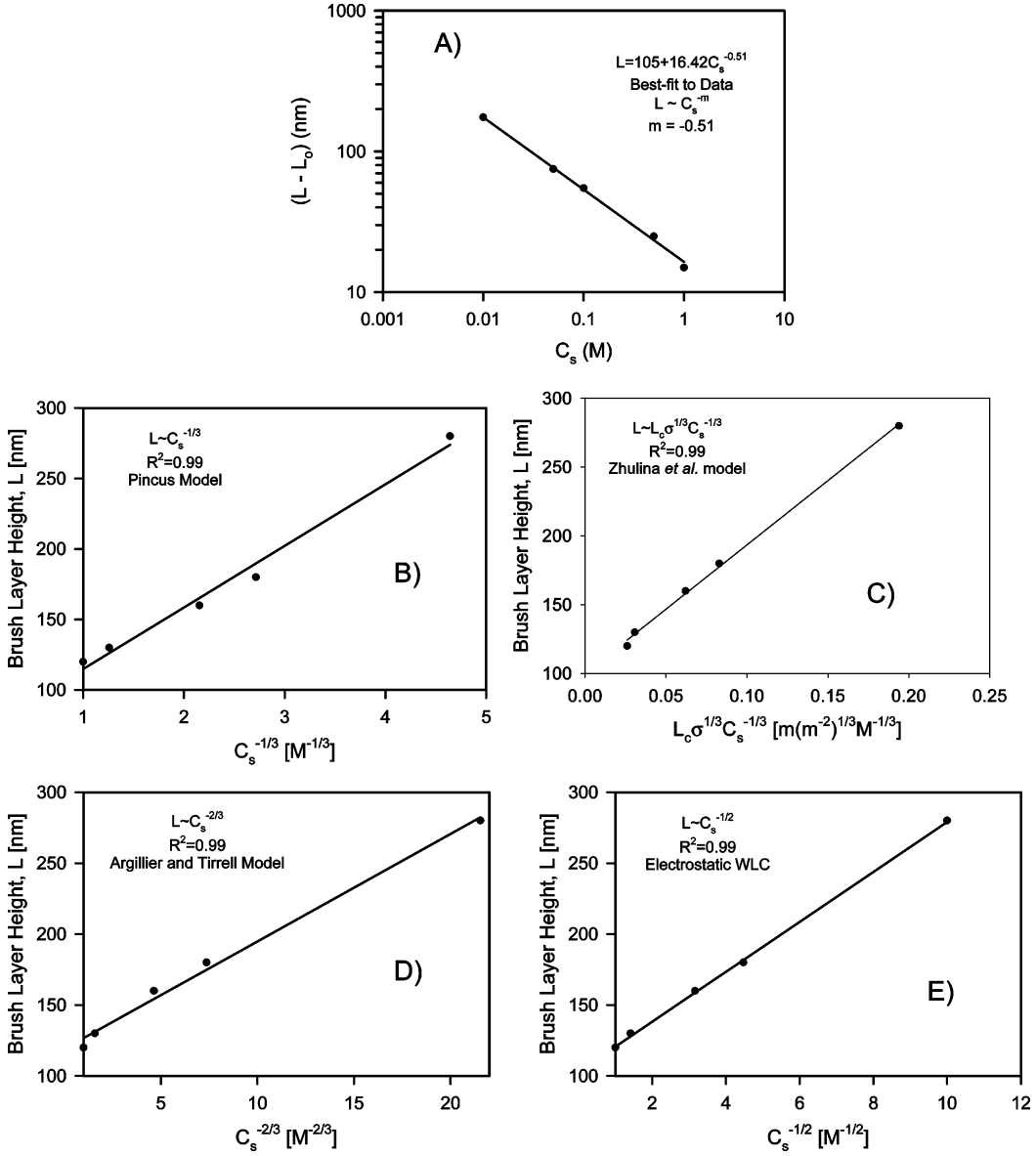

Figure 6. Scaling relationships between L and C_S for polyelectrolytes. (A) The general power law relationship ($L \sim C_S^{-m}$) describes the dependence of brush thickness on added salt concentration, where $m = 0.51$. Plots B−E represent different relationships that have been proposed for polyelectrolytes. (B) Pincus model,[72] (C) Zhulina et al.[73] model, (D) Argillier and Tirrel[75] model, and (E) Electrostatic WLC model.[77,78]

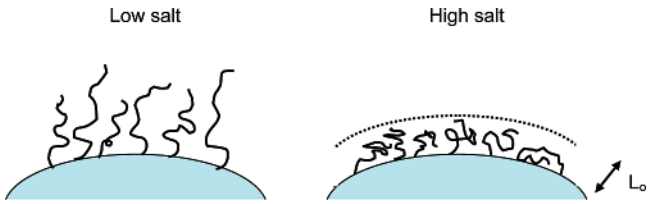

Figure 7. Conceptual representation of the conformation of bacterial surface biopolymers at low and high salt concentrations.

tinue to increase the salt concentration in solution, the most we could compress the brush layer is to a height of 105 nm. We measured a maximum compression of the brush layer as 120 nm in 1 M KCl (Table 2), but the model implies that even as the salt concentration is increased further, the brush layer could not collapse to a height <105 nm (Figure 7).

Effect of Ionic Strength on Biopolymer Adhesion. A distribution of adhesion peaks between the AFM tip and the bacterial surface polymers was observed in all solvents (Figure 8), which mainly reflects the heterogeneity of the bacterial surface. If an average value for the force over all of the measured adhesion events was used to represent the adhesion force at a given salt concentration, then a comparison could be made between the adhesion force and C_S (Figure 9). Pairwise statistical tests were used to determine if the different "treatments" were significantly different from one another. All combinations of pairs among the six salt concentrations were tested. The average adhesion force at a given C_S was significantly different from the adhesion forces at all other salt concentrations except for the adhesion forces in water and 0.01 M KCl. The latter two treatments (water and 0.01 M KCl) were not significantly different from one another according to the Dunn rank sum test ($p > 0.05$).

Discussion

Effect of Ionic Strength on Biopolymer Conformation. For neutral polymer brushes on a solid surface, short-range intermolecular repulsion causes the chains to partially stretch in the direction normal to the grafting surface.[46,47] Polyelectrolyte brushes also stretch in the direction normal to the

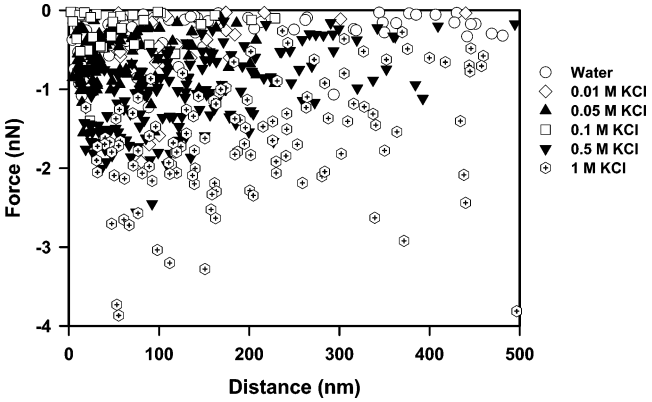

Figure 8. Distribution of adhesion forces observed between the silicon nitride AFM tip and *P. putida* KT2442 biopolymers as a function of ionic strength. Each data point represents an adhesion event between the tip and bacterial surface biopolymers as measured in the retraction portion of a force-displacement curve. Each retraction curve captured may have single or multiple adhesion events. The magnitude of the adhesion force is taken as the maximum value of each adhesion peak. Adhesion peaks were collected from the retraction portions of 25 different force-displacement curves, measured on five different bacterial cells for each salt concentration studied. The magnitude of each adhesion peak is shown in this figure. In some subsequent calculations, an average value was used to characterize the adhesive interaction at a given salt concentration.

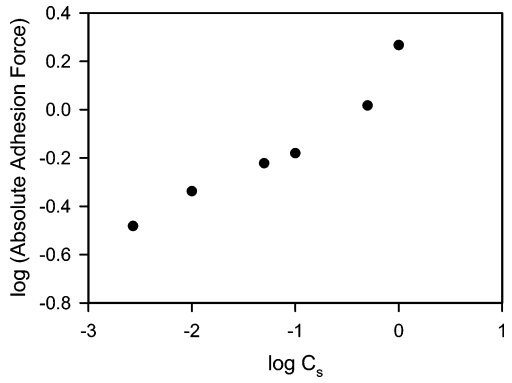

Figure 9. Relationship between measured adhesion force and added salt concentration. Each point represents an average of all the adhesion peaks for a given salt concentration (all individual data points are shown in Figure 8).

grafting surface, but the stretching is caused primarily by electrostatic interactions in the layer instead of short-range repulsion between individual units of the molecule.[68,72] Because electrostatic interactions are long-range in nature, the chains can become stretched at lower grafting densities, below the overlapping threshold.[68,69] Scaling relationships to describe the conformational behavior of grafted polyelectrolytes have been developed for planar and curved surfaces.[69−72] To our knowledge, such models have not been previously applied to macromolecules grafted to a microbial cell.

The microscopic (single molecule) investigation of polymer rigidity showed that the polymers were flexible under all conditions tested, and we did not observe a trend in the Kuhn length as a function of ionic strength. This implies that, for the polymers on the surface of *P. putida* KT2442, interactions between neighboring particles did not lead to electrostatic stiffening of the chains. This finding is consistent with the behavior of polyelectrolytes with a flexible backbone.[69] Previous experimental evidence also indicated that these biopolymers are flexible in many solvents.[17,27]

Polyelectrolyte Theories. The observed scaling relationship of the brush layer height (L) with $L_c(\Gamma v/l_k)^{1/3}$, as well as the failure of the relation for an uncharged brush $L/l_k \sim (\Gamma l_k^2)^{1/3}$, confirms that the biopolymer layer is charged, consistent with the behavior of a polyelectrolyte brush. Neutral and charged polymers can be described using the "blob" model,[47] in which a chain at an interface is viewed as a succession of noninteracting blobs. A chain within one blob assumes a conformation that is equivalent to that in a dilute polymer solution. Monomers can interact with adjacent and distant segments in their blob, but not with segments from other blobs. Interactions in a blob can be described by the segment or Kuhn length (l_k) and the reduced excluded volume (v/l_k^3). For neutral polymers, the segment length is independent of polymer−solvent affinity, but for polyelectrolytes, both the segment length and the excluded volume may be affected by electrostatic interactions.

The concept of an electrostatic wormlike chain has been developed, in which changes in ionic strength affect the local chain stiffness and the excluded volume. Fixman et al.[77,78] accounted for electrostatic effects within a segment by modeling the backbone of the polymer as a charged torus and solving the nonlinear Poisson−Boltzmann expression for the electrostatic field. Electrostatic and steric hindrances were balanced against the kinetic energy of the chain, and expressions were developed to describe the relationship between salt concentration and chain conformation. Hariharan et al.[70] showed that adoption of the electrostatic wormlike chain theory provides the scaling relationship $L \sim C_s^{-1/2}$. In our study, the brush layer height scaled with $C_s^{-1/2}$, but other relationships could not be ruled out. An alternate treatment of local chain stiffening and excluded volume effects by Argillier and Tirrell suggested that polyelectrolytes scale according to the relationship $L \sim C_s^{-2/3}$.[75] A theory developed by Zhulina et al.[73] that is applicable to both salted and unsalted polyelectrolyte brushes expresses the free energy function as the sum of entropic interactions at a given temperature and the energy caused by excluded volume interactions and incorporates both electrostatic and nonelectrostatic effects. For the salted brush, the scaling relationship obtained is $L \sim L_c\Gamma^{1/3}C_s^{-1/3}$. Both of these latter two relationships described our data nearly as well as that of the electrostatic wormlike chain model.

Although each of the scaling theories (electrostatic wormlike chain, Argillier and Tirrell's treatment of chain stiffening, and Zhulina et al.'s models for a salted brush) reasonably explained the relationship between the brush layer height and the salt concentration, other evidence suggests that the electrostatic wormlike chain model is not applicable to these biopolymers. The Kuhn length was nearly insensitive to salt concentration, and so chain stiffening does not appear to have been a factor in influencing biopolymer conformation.

Balance of Attractive and Repulsive Forces. A transition in the adhesion force was seen between a C_s of 0.1 and 0.5 M (Table 3). Above a critical salt concentration, the net concentration of ions in the solvent exceeds the net concentration of ions in the polymer brush. A theoretical investiga-

Table 3. Comparison of Measured Adhesion Forces with DLVO Predictions as a Function of Added Salt Concentration

C_s (M)	predicted electrostatic repulsion[b] (nN)	predicted force (electrostatic + van der Waals[c] + Born repulsion[d]) (nN)	average adhesion force (measured) (nN)
water	3.85	2.96	−0.33
0.01	2.07	1.18	−0.46
0.05	0.46	−0.43	−0.60
0.10	0.15	−0.74	−0.66
0.50	0.04	−0.85	−1.04
1.00	0.05	−0.84	−1.85

[a] By convention for AFM data, attractive forces are negative and repulsive forces are positive in sign. [b] Predicted based on sphere-sphere interaction force calculated at a separation distance of 0.3 nm. [c] van der Waals interactions were calculated for sphere−sphere geometry, assuming a separation distance of 0.3 nm and were −3.09 nN, insensitive to salt concentration. [d] Born repulsive forces were calculated for sphere-sphere geometry, assuming a separation distance of 0.3 nm and were 2.20 nN, insensitive to salt concentration (C_s).

Table 4. Summary of Physical Property Transitions as a Function of Added Salt Concentration

Transition occurs between water and 0.01 M KCl
Kuhn length (l_k is significantly different between water and 0.01 M KCl; l_k's are not significantly differently between 0.01 M KCl and all higher salt concentrations)

Transition occurs between 0.01 and 0.05 M KCl
Electrophoretic mobility
Softness of the bacterial surface (the slopes of the compliance regions in water and 0.01 M KCl were not significantly different from one another but they are each different from the rest of the data)

Transition occurs between 0.05 and 0.10 M KCl
Predicted energy barrier based on soft-particle DLVO theory (attraction observed at > 0.05 M KCl)

Transition occurs between 0.1 and 0.5 M KCl
Magnitude of the average adhesion force between biopolymers and AFM tip

tion of how the energy barriers change with salt concentration based on the use of soft-particle DLVO theory showed that for a salt concentration >0.05 M, the total interaction energy was attractive (Table 1, Figure 2).

Adhesion between two bodies is primarily caused by van der Waals interactions when the bodies are uncharged. The adhesion between two spherical bodies can be calculated based on van der Waals interactions as

$$F_v = \frac{A}{6H_o^2}\left(\frac{a_1 a_2}{a_1 + a_2}\right) \quad (9)$$

where H_o the distance of closest approach, usually assumed to be 0.3 nm.[83] It is not necessary to consider retardation effects at this short distance. Application of eq 12 provides an adhesion force of 3.09 nN at all salt concentrations (Table 3), because van der Waals interactions are typically considered to be independent of ionic strength.[7]

The attraction of the polymer for the tip is balanced by electrostatic and Born repulsion, as well as the stretching energy of the chain as the AFM tip is retracted. We estimated the amount of electrostatic repulsive forces between the bacterium and the tip at 0.3 nm by applying the relation $dE_e/dh = -F_e$ where E_e was calculated in eq 8. The electrostatic force between two dissimilar spheres at a separation distance H_o can be written as

$$F_e = -\frac{4\pi a_1 a_2 n k_B T}{(a_1 + a_2)\kappa}(\Phi_1^2 + \Phi_2^2)\left[e^{-2\kappa H_o} - \frac{2\Phi_1\Phi_2}{\Phi_1^2 + \Phi_2^2}e^{-\kappa H_o}\right]\left[\frac{1}{1 - e^{-2\kappa H_o}}\right] \quad (10)$$

The electrostatic forces as a function of C_s are shown in Table 3.

Born repulsion is a strong short-range repulsion that originates from the repulsive forces between atoms as their shells interpenetrate each other. A Hamaker-type integration for all molecules in the systems was developed by Feke et al.[84] for the Born repulsive energy between two spheres. Detailed expressions are provided in the Appendix.

We previously ignored Born repulsion in the calculation of DLVO energy profiles between the bacterium and the tip because such forces are only important at very short separations. However, when we consider the closest possible separation distance of 0.3 nm, the Born repulsion must be included. The calculated Born repulsive force for $h = H_o =$ 0.3 nm was 2.20 nN, irrespective of the salt concentration.

The net interaction force at each salt concentration was calculated as the sum of van der Waals attractions, electrostatic repulsion, and Born repulsion. The sum of these forces was compared with the measured adhesion force in each salt solution (Table 4). In water and 0.01 M KCl, the predicted adhesion was higher than the average experimentally measured adhesion. In the other four solutions, the predicted and measured adhesion values were similar.

Our simple force balance comes surprisingly close to predicting the measured adhesion forces but is not without limitations. One complicating factor is that the polyelectrolyte layer itself can increase the ionic strength of the solution in the area between the bacterium and the surface. Boonaert et al.[85] suggested that extracellular material released by *Lactococcus lactis* increased cellular adhesion to polystyrene and glass by increasing the ionic strength of the solution in the region confined between the cells and the substrate. If the local ionic strength was higher, electrostatic repulsion would be less than we predicted.

The forces we calculated in the force balance also did not include hydrogen bonds and the energy of the chain stretching, which would also each contribute to measured adhesion. The actual adhesion force reflects a combination of van der Waals attraction, Born repulsion, chain stretching energy, hydrogen bonding, and electrostatic repulsion. The difficulty in making the force balance reemphasizes the complex nature of the bacterial surface and further necessitates the need for detailed molecular studies of bacterial surface properties.

Critical Salt Concentrations Influencing Biopolymer Conformation and Adhesion. For each physicochemical property that was probed, a transition occurred that was dependent on the salt concentration (Table 4). In pure water, the biopolymer layer was extended, "soft", showed low

adhesion, exhibited a highly negative electrophoretic mobility and large energy barrier to adhesion, and corresponded to a random conformation. As the salt concentration increased, these physical properties were modified.

Above 0.01 M, the bacterial surface layer transitioned toward a more rigid and ordered structure, the electrophoretic mobility began to reach a plateau, and the predicted energy profile (at $C_s > 0.05$ M) changed from repulsive to attractive. The magnitude of the adhesion force underwent a transition between 0.1 and 0.5 M KCl, shifting toward higher adhesion between the biopolymers and the AFM tip. Most physical properties were similar in 0.5 and 1 M KCl. At these two latter salt concentrations, the polymer brush layer can be considered rigid (although individual polymers are still flexible), the adhesion forces are high, the electrophoretic mobility is less negative and not dependent on C_s, and attractive energy profiles are predicted.

Similar effects for some of these properties have been observed in other systems. For example, the exopolymer produced by *Pseudomonas* "gingeri" Pf9 became more rigid at higher ionic strengths because screening of negative charges on the polysaccharide chain promoted a transition toward a more rigid conformation.[86] Compression to a rigid fibrillar layer upon the addition of 0.1 M KCl was observed by van der Mei et al. when the surface of a fibrillated *Streptococcus salivarius* strain was probed via AFM.[80] In addition to experimental measurements, modeling has shown that the predicted DLVO energy profiles between wild type *Escherichia coli* and glass decreased from an energy barrier of ~420 k_BT in 0.02 M phosphate buffer to an attractive profile in 0.2 M phosphate buffer.[13] No other study addressed the combined effects of biopolymer conformation, brush layer properties, and DLVO forces on bacterial adhesion.

The conformation of biopolymers on a bacterial surface has not been greatly studied, but many studies addressed the role of salt concentration on conformation in systems of pure polysaccharides. For example, the anionic polysaccharide succinoglycan undergoes a salt-induced conformational transition from single chains in low salt solutions to dimers of associated single helices in higher salt solutions.[87−89] Xanthan undergoes a similar transition in that the triple helix can unravel if sufficient salt is not present in solution.[90−92] It is therefore not surprising to see salt-induced conformational changes in the biopolymers on the surface of *P. putida* KT-2442, based on the many studies of pure polysaccharides in solution.

Our studies suggest that electrostatic interactions affect the behavior of charged biopolymers in ways beyond what can be described by DLVO theory. Electrostatic interactions affect the conformation of the biopolymers and the softness of the bacterial polymer layer, and these properties in turn affect adhesion. Understanding the interplay of electrostatic and steric interactions in influencing the adhesion of bacteria to surfaces will be critical to the development of improved models predicting bacterial adhesion.

Summary

The biopolymers on the surface of *P. putida* KT2442 undergo a salt-induced conformational change from a soft, random structure in low ionic strength solutions to an ordered, rigid structure in the presence of salt. This conformational change occurs between 0.01 and 0.05 M KCl. Accompanying this conformational change, the adhesion behavior of the polymer changes. Greater adhesion forces are observed between the biopolymer and silicon nitride for the more rigid and charged brush layer in high ionic strength solutions. The change from repulsive to attractive interactions upon the addition of salt was predicted by soft-particle DLVO theory. This study provides evidence that conformational changes in biopolymers that occur due to the salt concentration in solution are important factors in influencing adhesion, and therefore, they need to be included in predictive models of bioadhesion.

Acknowledgment. We thank Dr. Patrick Guenoun for helpful discussions that provided the impetus for parts of this study. This publication was made possible in part by a CAREER Award to T.A.C. from the National Science Foundation (Grant Number BES-0238627).

Appendix

Soft-Particle DLVO Theory. The equations below show the dependence on ionic strength of several parameters which appear in the electrophoretic mobility expression (eq 2)

$$\Psi_o = \frac{k_B T}{ze}\left(\ln\left\{\frac{ZN}{2zn} + \left[\left(\frac{ZN}{2zn}\right)^2 + 1\right]^{1/2}\right\} + \frac{2zn}{ZN}\left\{1 - \left[\left(\frac{ZN}{2zn}\right)^2 + 1\right]^{1/2}\right\}\right) \quad \text{(A.1)}$$

$$K_m = \kappa\left[1 + \left(\frac{ZN}{2zn}\right)^2\right]^{1/4} \quad \text{(A.2)}$$

$$\kappa = \left(\frac{1}{\epsilon_o \epsilon k_B T}\sum_{i=1}^{N} z_i^2 e^2 n\right)^{1/2} \quad \text{(A.3)}$$

$$\Psi_{DON} = \frac{K_B T}{ze}\ln\left\{\frac{ZN}{2zn} + \left[\left(\frac{ZN}{2zn}\right)^2 + 1\right]^{1/2}\right\} \quad \text{(A.4)}$$

where z is the valence of bulk ions, n is the concentration of bulk ions, and κ is the Debye screening length. The parameter ZN represents spatial charge density in the polyelectrolyte region, and the term $1/\lambda_s$ characterizes the softness of the bacterial surface. The electrophoretic mobility is measured as a function of salt concentration and these data is used to fit the parameters ZN and $1/\lambda_s$ from eq 2 in the text.

Born Repulsive Interactions. Born repulsion is a strong short-range repulsion that originates from the repulsive forces between atoms as their shells interpenetrate one another. A Hamaker-type integration for all molecules in the systems was developed by Feke et al.[84] for the Born repulsive energy between two spheres. The equations describing such interactions are as follows:

$$E_b = A_1 A_2 \quad \text{(A.5)}$$

$$A_1 = 4A\left(\frac{\sigma}{a_1}\right)^{n-6}\frac{(n-8)!}{(n-2)!}\frac{1}{R} \quad \text{(A.6)}$$

and

$$A_2 = \left[\frac{-R^2-(n-5)(\lambda-1)R-(n-6)[\lambda^2-(n-5)\lambda+1]}{(R-1+\lambda)^{n-5}}+\frac{-R^2+(n-5)(\lambda-1)R-(n-6)[\lambda^2-(n-5)\lambda+1]}{(R+1-\lambda)^{n-5}}+\frac{R^2+(n-5)(\lambda+1)R+(n-6)[\lambda^2+(n-5)\lambda+1]}{(R+1+\lambda)^{n-5}}+\frac{R^2-(n-5)(\lambda+1)R+(n-6)[\lambda^2+(n-5)\lambda+1]}{(R-1-\lambda)^{n-5}}\right] \quad \text{(A.7)}$$

where R is the center-to-center separation distance made dimensionless on a_1 ($R = (a_1 + h + a_2)/a_1$), $\lambda = a_2/a_1$, and σ is the collision diameter (assumed to be 0.5 nm). The most common form of the expression is where $n = 12$. Using this value for n, the repulsive force was calculated by taking the negative derivative of the energy. The full expression for the Born repulsive forces between two spheres can be derived based on these equations ($n = 12$) as

$$F_B = -\frac{dE_b}{dh} = \frac{1}{a_1}\frac{dE_b}{dR} = \frac{1}{a_1}\left[A_1\frac{dA_2}{dR} + A_2\frac{dA_1}{dR}\right] \quad \text{(A.8)}$$

where

$$\frac{dA_1}{dR} = \frac{-4A}{151\,200R^2}\left(\frac{\sigma}{a_1}\right)^6 \quad \text{(A.9)}$$

$$\frac{dA_2}{dR} = \left[\frac{A_7{}^7(-2R-7(\lambda-1))-7A_3A_7{}^6}{A_7{}^{14}}+\frac{A_8{}^7(-2R+7(\lambda-1))-7A_4A_8{}^6}{A_8{}^{14}}+\frac{A_9{}^7(2R+7(\lambda+1))-7A_5A_9{}^6}{A_9{}^{14}}+\frac{A_{10}{}^7(2R-7(\lambda+1))-7A_6A_{10}{}^6}{A_{10}{}^{14}}\right] \quad \text{(A.10)}$$

$$A_3 = -R^2 - 7(\lambda-1)R - 6(\lambda^2-7\lambda+1) \quad \text{(A.11)}$$

$$A_4 = -R^2 + 7(\lambda-1)R - 6(\lambda^2-7\lambda+1) \quad \text{(A.12)}$$

$$A_5 = R^2 + 7(\lambda+1)R + 6(\lambda^2+7\lambda+1) \quad \text{(A.13)}$$

$$A_6 = R^2 - 7(\lambda+1)R + 6(\lambda^2+7\lambda+1) \quad \text{(A.14)}$$

$$A_7 = R - 1 + \lambda \quad \text{(A.15)}$$

$$A_8 = R + 1 - \lambda \quad \text{(A.16)}$$

$$A_9 = R + 1 + \lambda \quad \text{(A.17)}$$

$$A_{10} = R - 1 - \lambda \quad \text{(A.18)}$$

Glossary

Nomenclature

a_1: tip radius (250 nm)
a_2: the radius of the bacterium (500 nm)
A: Hamaker constant for the interacting media (10^{-20} J)
C_s: salt concentration of the solvent (M KCl)
e: electron charge (1.602×10^{-19} C)
E_b: Born repulsive energy (k_BT)
E_e: electrostatic interactions (k_BT)
E_t: total interaction energy (estimated by DLVO theory) (k_BT)
E_v: London−van der Waals interactions (k_BT)
F_{chain}: force required to stretch FJC chain to length h (nN)
F_e: electrostatic force between dissimilar spheres (nN)
F_{st}: steric force (nN)
F_v: van der Waals Interactions (nN)
h: separation distance between tip and biopolymers (nm)
H_o: distance of closest approach (0.3 nm)
k_B: Boltzmann constant (1.381×10^{-23} J/K)
K: constant with value of 1
K_m: Debye−Hückel parameter for the polymer layer
L: equilibrium height of the polyelectrolyte brush layer (m)
$\boldsymbol{L}^{-1}$: inverse Langevin function
L_c: contour length (1.25 L) used in scaling relationships (nm)
l_c: contour length obtained from FJC model (nm), represents a portion of whole chain length
l_k: Kuhn length (nm)
L_o: maximum compressed brush thickness (105 nm)
m: fractional exponent in polymer scaling model (0.51)
n: concentration of bulk ions (M)
N: density of the charged groups
R: center-to-center distance between two dissimilar spheres, made dimensionless by dividing by a_1
T: temperature (298 K)
Z: valance of the charged groups in the polymers
z: valence of bulk ions
Γ: grafting density of bacterial surface biopolymers in brush layer (m^{-2})
ϵ: permittivity of a vacuum (8.85×10^{-12} C^2/J m)
ϵ_o: relative permittivity of solvent (78 for water)
η: solvent viscosity (8.9×10^{-4} kg/m s)
κ: Debye screening length (nm)
λ: ratio between the sphere diameters (a_2/a_1)
λ_c: characteristic wavelength of the van der Waals interaction (100 nm)
λ_s: softness parameter (nm^{-1})
μ: electrophoretic mobility (m^2/V s)
ν: excluded volume (m^3)
σ: collision diameter (0.5 nm)
Φ_1: reduced potential of tip ($\Phi_1 = ze\psi_1/k_BT$)
Φ_2: reduced potential of bacterium ($\Phi_2 = ze\psi_2/k_BT$)
ψ_1 or ψ_{tip}: surface potential of tip (V)
ψ_2 or $\psi_{bacterium}$: surface potential of bacterium (V)
Ψ_{DON}: Donnan potential of polymer layer (V)
Ψ_o: surface zeta potential (V)

References and Notes

(1) Williams, V.; Fletcher, M. *Appl. Environ. Microbiol.* **1996**, *62*, 100.
(2) DeFlaun, M. F.; Oppenheimer, S. R.; Streger, S.; Condee, C. W.; Fletcher, M. *Appl. Environ. Microbiol.* **1999**, *65*, 759.
(3) Simoni, S. F.; Harms, H.; Bosma, T. N. P.; Zehnder, A. J. B. *Environ. Sci. Technol.* **1998**, *32*, 2100.

(4) Triandafillu, K.; Balazs, D. J.; Aronsson, B.-O.; Descouts, P.; Tu Quoc, P.; van Delden, C.; Mathieu, H. J.; Harms, H. *Biomaterials* **2003**, *24*, 1507.
(5) Henriksson, A.; Szewzyk, R.; Conway, P. L. *Appl. Environ. Microbiol.* **1991**, *57*, 499.
(6) Marshall, K. C.; Stout, R.; Mitchell, R. *J. General Microbiol.* **1971**, *68*, 337.
(7) Israelachvili, J. N. *Intermolecular & Surface Forces*, 2nd ed.; Academic Press: New York, 1992.
(8) Rijnaarts, H. H. M.; Norde, W.; Lyklema, J.; Zehnder, A. J. B. *Colloids Surf. B: Biointerfaces* **1999**, *14*, 179.
(9) Zita, A.; Hermansson, M. *Appl. Environ. Microbiol.* **1994**, *60*, 3041.
(10) Smets, B. F.; Grasso, D.; Engwall, M. A.; Machinist, B. J. *Colloids Surf. B: Biointerfaces* **1999**, *14*, 121.
(11) Poortinga, A. T.; Bos, R.; Busscher, H. J. *Colloids Surf. B: Biointerfaces* **2001**, *20*, 105.
(12) Abu-Lail, N. I.; Camesano, T. A. *Environ. Sci. Technol.* **2003**, *37*, 2173.
(13) McLaine, J. W.; Ford, R. M. *Appl. Environ. Microbiol.* **2002**, *68*, 1280.
(14) Dan, N. *Colloid Surf. B: Biointerfaces* **2003**, *27*, 41.
(15) van Oss, C. J. *Interfacial Forces in Aqueous Media*; Marcel Dekker: New York, 1994.
(16) Van der Aa, B. C.; Michel, R. M.; Asther, M.; Zamora, M. T.; Rouxhet, P. G.; Dûfrene, Y. F. *Langmuir* **2001**, *17*, 3116.
(17) Abu-Lail, N. I.; Camesano, T. A. *Langmuir* **2002**, *18*, 4071.
(18) Lower, S. K.; Tadanier, C. J.; Hochella, M. F., Jr. *Geochim. Cosmochim. Acta* **2000**, *64*, 3133.
(19) Lower, S. K.; Tadanier, C. J.; Hochella, M. F., Jr. *Geomicrobiol. J.* **2001**, *18*, 63.
(20) Lower, S. K.; Hochella, M. F., Jr.; Beveridge, T. J. *Science* **2001**, *292*, 1360.
(21) Ong, Y.-L.; Razatos, A.; Georgiou, G.; Sharma, M. M. *Langmuir* **1999**, *15*, 2719.
(22) Bowen, W. R.; Lovitt, R. W.; Wright, C. J. *J. Colloid Interface Sci.* **2000**, *228*, 428.
(23) Vigeant, M. A. S.; Ford, R. M.; Wagner, M.; Tamm, L. K. *Appl. Environ. Microbiol.* **2002**, *68*, 2794.
(24) Prince, J. L.; Dickinson, R. B. *Langmuir* **2003**, *19*, 154.
(25) Camesano, T. A.; Unice, K. M.; Logan, B. E. *Colloids Surf. A: Physicochem. Eng. Aspects* **1999**, *160*, 291.
(26) Camesano, T. A.; Logan, B. E. *Environ. Sci. Technol.* **2000**, *34*, 3354.
(27) Camesano, T. A.; Abu-Lail, N. I. *Biomacromolecules* **2002**, *3*, 661.
(28) Ramos-Diaz, M. A.; Ramos, J. L. *J. Bacteriol.* **1998**, *180*, 6352.
(29) Eberl, L.; Ammendola, A.; Rothballer, M. H.; Givskov, M.; Sternberg, C.; Kilstrup, M.; Schleifer, K.-H.; Molin, S. *Appl. Environ. Microbiol.* **2000**, *182*, 3368.
(30) Pérez-Pantoja, D.; Guzmán, L.; Manzano, M.; Pieper, D. H.; González, B. *Appl. Environ. Microbiol.* **2000**, *66*, 1602.
(31) Klemba, M.; Jakobs, B.; Wittich, R.-M.; Pieper, D. *Appl. Environ. Microbiol.* **2000**, *66*, 3255.
(32) van der Meer, J. R.; van Neerven, A. R. W.; De Vries, E. J.; De Vos, W. M.; Zehnder, A. J. B *J. Bacteriol.* **1991**, *173*, 6.
(33) Nüsslein, K.; Maris, D.; Timmis, K.; Dwyer, D. F. *Appl. Environ. Microbiol.* **1992**, *58*, 3380.
(34) Vermette, P.; Meagher, L. *Langmuir* **2002**, *18*, 10137.
(35) Wissink, M. J. B.; Van Luyn, M. J. A.; Beernink, R.; Dijk, F.; Poot, A. A.; Engbers, G. H. M.; Beugling, T.; Van Aken, W. G.; Feijen, J. *Thrombosis Haemostasis* **2000**, *84*, 325.
(36) Lee, J. M.; Edwards, H. H. L.; Pereira, C. A.; Samii, S. I. *J. Mater. Sci.* **1996**, *7*, 531.
(37) Cleveland, J. P.; Manne, S.; Bocek, D.; Hansma, P. K. *Rev. Sci. Instrum.* **1993**, *64*, 403.
(38) Tomitori, M.; Arai, T. *Appl. Surf. Sci.* **1999**, *140*, 432.
(39) Ducker, W. A.; Senden, T. J.; Pashley, R. M. *Nature* **1991**, *353*, 239.
(40) Dufrêne, Y. F.; Boonaert, C. J. P.; van der Mei, H. C.; Busscher, H. J.; Rouxhet, P. G. *Ultramicroscopy* **2001**, *86*, 113.
(41) Boonaert, C. J. P.; Rouxhet, P. G.; Dufrêne, Y. F. *Surf. Interface Anal.* **2000**, *30*, 32.
(42) Van der Aa, B. C.; Dûfrene, Y. F. *Colloids Surf. B: Biointerfaces* **2002**, *23*, 173.
(43) Vadillo-Rodriguez, V.; Busscher, H. J.; Norde, W.; de Vries, J.; van der Mei, H. C. *Langmuir* **2003**, *19*, 2372.
(44) Yao, X.; Walter, J.; Burke, S.; Stewart, S.; Jericho, M. H.; Pink, D.; Hunter, R.; Beveridge, T. J. *Colloids Surf. B: Biointerfaces* **2002**, *23*, 213.
(45) Boulbitch, A. *J. Electron Microscopy* **2000**, *49*, 459.
(46) Alexander, S. *J. Phys. II (Paris)* **1977**, *38*, 983.
(47) de Gennes, P. G. *Adv. Colloid Interface Sci.* **1987**, *27*, 189.
(48) Butt, H.-J.; Kappl, M.; Mueller, H.; Raiteri, R. *Langmuir* **1999**, *15*, 2559.
(49) Drummond, C. J.; Senden, T. J. *Colloids Surf. A: Physicochem. Eng. Aspects* **1994**, *87*, 217.
(50) Senden, T. J.; Drummond, C. J. *Colloids Surf. A: Physicochem. Eng. Aspects* **1995**, *94*, 29.
(51) Ohshima, H. K. *J. Colloid Interface Sci.* **1989**, *130*, 281.
(52) Bos, R.; van der Mei, H. C.; Busscher, H. J. *Biophys. Chem.* **1998**, *74*, 251.
(53) Hayashi, H.; Tsuneda, S.; Hirata, A.; Sasaki, H. *Colloids Surf. B: Biointerfaces* **2001**, *22*, 149.
(54) Morisaki, H.; Nagai, S.; Ohshima, H.; Ikemoto, E.; Kogur, K. *Microbiology* **1999**, *145*, 2797.
(55) Takashima, S.; Morisaki, H. *Colloids Surf. B: Biointerfaces* **1997**, *9*, 205.
(56) Hogg, R.; Healy, T. W.; Fuerstenau, D. W. *Trans. Faraday Soc.* **1966**, *62*, 1638.
(57) Elimelech, M.; Gregory, J.; Jia, X.; Williams, R. A. *Particle deposition & aggregation: Measurement, modelling and simulation*; Butterworth-Heinemann: Woburn, MA, 1995.
(58) Zhmud, B. V.; Sonnefeld, J.; Bergstrom, L. *Colloids Surf. A: Physicochem. Eng. Aspects* **1999,** *158*, 327.
(59) Larson, I.; Pugh, R. J. *Langmuir* **1998**, *14*, 5676.
(60) Schenkel, J. H.; Kitchener, J. A. *Trans. Faraday Soc.* **1960**, *56*, 161.
(61) Martin, R. E.; Bouwer, E. J.; Hanna, L. M. *Environ. Sci. Technol.* **1992**, *26*, 1053.
(62) Grasso, D.; Smets, B. F.; Strevett, K. A.; Machinist, D. B.; van Oss, C. J.; Giese, R. F.; Wu, W. *Environ. Sci. Technol.* **1996**, *30*, 3604.
(63) Oritz, C.; Hadziioannotu, G. *Macromolecules* **1999**, *32*, 780.
(64) Butt, H.-J. *Biophys. J.* **1992**, *60*, 777.
(65) Milner, S. T.; Witten, T. A.; Cates, M. E. *Macromolecules* **1988**, *21*, 2610.
(66) Miklavic, S. J.; Marcelja, S. *J. Phys. Chem.* **1988**, *92*, 6718.
(67) Misra, S.; Varanasi, S.; Varanasi, P. P. *Macromolecules* **1989**, *22*, 4173.
(68) Borisov, O. V.; Birshtein, T. M.; Zhulina, E. B. *J. Phys. II* **1991**, *1*, 521.
(69) Borisov, O. V.; Zhulina, E. B.; Birshtein, T. M. *Macromolecules* **1994**, *27*, 4795.
(70) Hariharan, R.; Biver, C.; Mays, J.; Russel, W. B. *Macromolecules* **1998**, *31*, 7506.
(71) Hariharan, R.; Biver, C.; Russel, W. B. *Macromolecules* **1998**, *31*, 7514.
(72) Pincus, P. *Macromolecules* **1991**, *24*, 2912.
(73) Zhulina, E. B.; Borisov, O. V.; Birshtein, T. M. *J. Phys. II* **1992**, *2*, 63.
(74) Pincus, P. A.; Rossi, G.; Cates, M. E. *Europhys. Lett.* **1987**, *4*, 41.
(75) Argillier, J. F.; Tirrell, M. *Theor. Chim. Acta* **1992**, *82*, 343.
(76) Witten, T.; Pincus, P. *Europhys. Lett.* **1987**, *3*, 315.
(77) Fixman, M.; Skolnick, J. *Macromolecules* **1978**, *11*, 863.
(78) Fixman, M. *J. Chem. Phys.* **1990**, *92*, 6283.
(79) Biver, C.; Hariharan, R.; Mays, J.; Russel, W. B. *Macromolecules* **1997**, *30*, 1787.
(80) van der Mei, H. C.; Busscher, H. J.; Bos, R.; de Vries, J.; Boonaert, C. J. P.; Dufrêne, Y. F. *Biophys. J.* **2000**, *78*, 2668.
(81) Vongoeler, F.; Muthukumar, M. *Macromolecules* **1995**, *28*, 6608.
(82) Davis, R. M.; Russel, W. B. *J. Polym. Sci. Part B−Polym. Phys.* **1986**, *24*, 511.
(83) Rabinovich, Y. I.; Adler, J. J.; Ata, A.; Singh, R. K.; Moudgil, B. M.; *J. Colloid Interface Sci.* **2000**, *232*, 10.
(84) Feke, D. L.; Prabhu, N. D.; Mann, J. A., Jr.; Mann, J. A., III. *J. Phys. Chem.* **1984**, *88*, 5735.
(85) Boonaert, C. J. P.; Dufrene, Y. F.; Derclaye, S. R.; Rouxhet, P. G. *Colloids Surf. B: Biointerfaces* **2001**, *22*, 171.
(86) Gianni, R.; Cescutti, P.; Bosco, M.; Fett, W. F.; Rizzo, R. *Int. J. Biol. Macromolecules* **1999**, *26*, 249.
(87) Balnois, E.; Stoll, S.; Wilkinson, K. J.; Buffle, J.; Rinaudo, M.; Milas, M. *Macromolecules* **2000**, *33*, 7440.
(88) Borsali, R.; Rinaudo, M.; Noirez, L. *Macromolecules* **1995**, *28*, 1085.
(89) Burova, T. V.; Golubeva, I. A.; Grinberg, N. V.; Mashkevich, A. Y.; Grinberg, V. Y.; Usov, A.; Navarini, L.; Cesaro, A. *Biopolymers* **1996**, *39*, 517.
(90) Camesano, T. A.; Wilkinson, K. J. *Biomacromolecules* **2001**, *2*, 1184.
(91) Holzwarth, G. *Biochemistry* **1976**, *15*, 4333.
(92) Holzwarth, G.; Prestridge, E. B. *Science* **1977**, *197*, 757.

BM034055F